

Nanoscale

Accepted Manuscript



This is an *Accepted Manuscript*, which has been through the Royal Society of Chemistry peer review process and has been accepted for publication.

Accepted Manuscripts are published online shortly after acceptance, before technical editing, formatting and proof reading. Using this free service, authors can make their results available to the community, in citable form, before we publish the edited article. We will replace this *Accepted Manuscript* with the edited and formatted *Advance Article* as soon as it is available.

You can find more information about *Accepted Manuscripts* in the [Information for Authors](#).

Please note that technical editing may introduce minor changes to the text and/or graphics, which may alter content. The journal's standard [Terms & Conditions](#) and the [Ethical guidelines](#) still apply. In no event shall the Royal Society of Chemistry be held responsible for any errors or omissions in this *Accepted Manuscript* or any consequences arising from the use of any information it contains.

COMMUNICATION

Dual-radiolabeled nanoparticle SPECT probes for bioimaging

Cite this: DOI: 10.1039/x0xx00000x

Kvar C.L. Black¹, Walter J. Akers¹, Gail Sudlow¹, Baogang Xu¹, Richard Laforest¹, Samuel Achilefu^{1,2,3*}

Received 10th September 2014,

¹Departments of Radiology, ²Biomedical Engineering, and ³Biochemistry & Molecular Biophysics, Washington University in St. Louis, Missouri 63110, USA.

DOI: 10.1039/x0xx00000x

www.rsc.org/

*Corresponding author: achilefus@mir.wustl.edu

A gold nanoparticle was radiolabeled with ¹²⁵I and ¹¹¹In and functionalized with an MMP9-cleavable peptide to form a multispectral SPECT imaging contrast agent. Peptide cleavage from the nanoprobe by MMP9 was observed *in vitro*, and distinct pharmacokinetic properties of the contrast agent were observed between tumors with high or low MMP9 expression.

With proper design, nanoparticles (NPs) offer multifunctional properties that can be harnessed for both diagnostic and therapeutic biomedical applications.¹ Due to their localized surface plasmon resonant (LSPR) properties, gold NPs^{2, 3} in particular offer unique optical properties that can be used for imaging⁴ or photothermal therapy⁵ of either cancerous⁶ or bacterial⁷ cells. Incorporating radioactive functionality into NPs⁸ is an emerging strategy to quantitatively evaluate their *in vivo* performance with quantitative biodistribution and imaging modalities such as positron emission tomography (PET)^{9, 10} and optical Cerenkov imaging.^{4, 11} Distinct from PET that only detects 511 keV gamma ray pairs, single photon emission computed tomography (SPECT) has the ability to detect a range of photonic energies, and therefore can be employed in multispectral imaging using multiple radionuclides. When properly integrated with NP probes, this independent tracking can help characterize important *in vivo* parameters such as radiolabeling stability, surface anchor stability, and biological parameters such as enzyme activity.

In this study, a multifunctional NP agent was designed to passively target tumors and characterize matrix metalloproteinase

(MMP) activity using a dual-radiolabeling strategy. The strategy takes inspiration from optically-activatable probes used to image enzyme activity,¹²⁻¹⁴ and it involves the synthesis of an imaging agent containing two distinct radionuclides separated by a cleavable linker,¹⁵ whose gamma emissions can be spectrally differentiated. The surface of gold nanoparticles was functionalized with a peptide (pMMP9; sequence: DTPA-Gly-Pro-Leu-Gly-Val-Arg-Gly-Lys-Gly-Tyr-Gly-Ahx-Cys-NH₂) containing four important components:

(1) a sequence which is cleaved specifically between the Leu and Gly residues in the presence of MMP9, (2) a tyrosine residue to radiolabel with ¹²⁵I, (3) a DTPA chelator to radiolabel with radiometals (⁶⁴Cu and ¹¹¹In), and (4) a cysteine residue to anchor to the gold surface. In addition, polyethylene glycol (PEG) was incorporated onto the NP surface, which was necessary to stabilize the peptide-functionalized NP suspension in aqueous environments (Figure S1). The pMMP9/PEG ratio was ~ 1.4, corresponding to 16 peptides and 11 PEG molecules per NP.

Once surface-functionalized with the cleavable peptide and PEG, an experiment was performed in PBS in order to characterize the ability of MMP9 to cleave the peptide present on the nanoparticle surface. In this experiment, ⁶⁴Cu was chelated to DTPA on the peptide attached to the NP. The suspension was incubated with MMP9 for 1.5 hours and then the supernatant solution was separated from the NPs by centrifugal filtration. Importantly, 23% of the radioactivity was observed in the supernatant after incubation with MMP9 compared to less than 5% in a control without MMP9 (Figure S2), which is attributed to the presence of ⁶⁴Cu-labeled

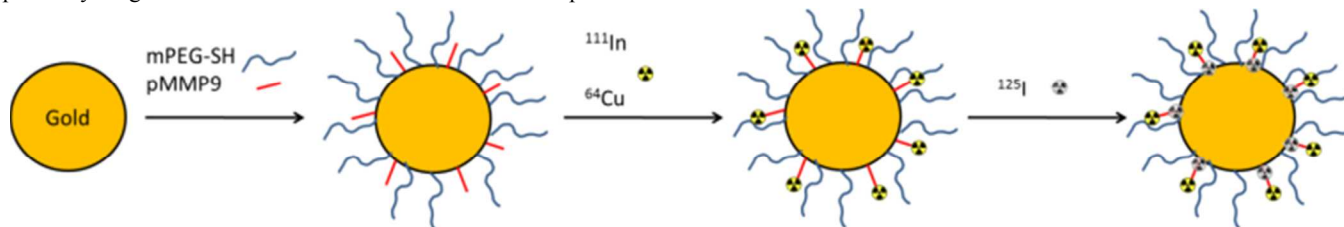


Figure 1. Schematic of the synthesis of the dual-radiolabeled nanoparticle-based SPECT probes, composed of a gold nanoparticle core, a peptide that could be radiolabeled with radiometals as well as radiohalogens separated by an MMP9-cleavable peptide sequence, and methoxy polyethylene glycol.

peptide fragments cleaved from the NP by MMP9. To further confirm the presence of the cleaved peptide, high performance liquid chromatography (HPLC) was performed on the supernatant solutions, and co-registered UV and radioactive peaks associated with the radiolabeled peptide fragment were observed (Figure S3).

For *in vivo* spectroscopic SPECT imaging, peptide-functionalized NPs were dual radiolabeled with ^{111}In and ^{125}I . The NP was radiolabeled in two successive steps (Figure 1). First $^{111}\text{InCl}_3$ was added to a pellet of the surface-functionalized NP in an acidic buffer under mild heating (45 °C) and incubated for one hour, resuspended in PBS buffer, and centrifuged to remove unchelated ^{111}In . Radiochemical purity of the pellet was characterized with thin layer chromatography (TLC) and confirmed to be >95%. Then the pellet suspended in PBS was added to an iodogen tube and incubated with Na^{125}I for one hour. Once again, TLC was performed to ensure radiochemical purity greater than 95%. The $^{125}\text{I}/^{111}\text{In}$ activity ratio of the sample was 0.6, corresponding to 15 ^{125}I atoms and 1 ^{111}In atom per NP since the specific activity of ^{111}In is 24X greater than that of ^{125}I .

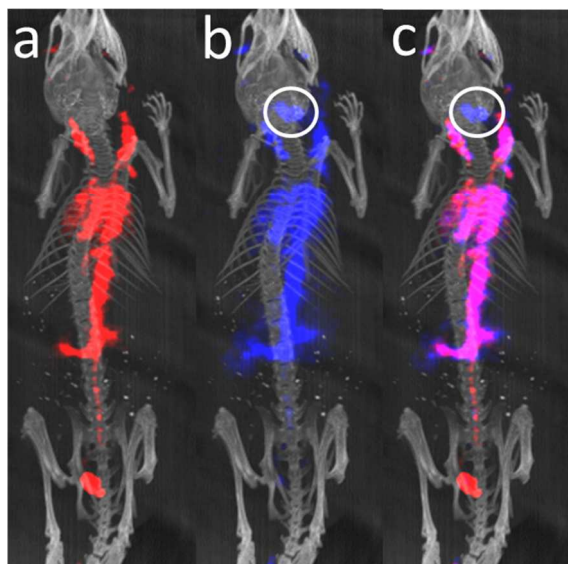


Figure 2. *In vivo* spectroscopic SPECT/CT imaging after intravenous injection with dual-radiolabeled nanoparticles. X-ray CT coregistered with (a) 200 ± 60 keV energy channel that detects ^{111}In , (b) 28 ± 3 keV energy channel that detects ^{125}I emission, and (c) both energy channels. Visible thyroid accumulation in the ^{125}I channel is circled.

Next, a phantom study was performed on the multifunctional NP suspension in order to confirm the spectroscopic imaging capability with the dual-radiolabeled agent. The dual-radiolabeled suspension was imaged along with two controls containing only ^{111}In or ^{125}I . Two imaging windows were chosen to independently collect photonic emissions from ^{111}In and ^{125}I . More specifically, a narrow window centered at 28 keV was used to detect x-ray emissions from ^{125}I (colored blue), and a broad window centered around 200 keV was used to acquire gamma emissions from ^{111}In (colored red). As can be observed in Figure S4, the two control vials only appear as separate colors representing respective energy windows, while the dual-radiolabeled sample contains signal from both energy windows. When the two channels are merged, the NP sample appears purple due to the presence of both ^{125}I and ^{111}In .

To explore the *in vivo* pharmacokinetics and biodistribution of these multifunctional NPs, suspensions were intravenously injected into tumor-bearing mice and *in vivo* imaging was performed (Figure 2). Importantly, both ^{111}In and ^{125}I signals could be independently detected in the mice (Figure 2a and b), and were co-registered mainly in the blood pool, with the heart, carotid arteries, and descending aorta all clearly visible (purple signal seen in Figure 2c). In addition, ^{125}I was identified in the thyroid, and ^{111}In was observed in the bladder. Interestingly, 4 hours after injection, while the ^{111}In signal was still present mainly in the blood, the ^{125}I signal was isolated to the thyroid, stomach, and bladder (Figure S5). This result is attributed to functional *in vivo* stability of the ^{111}In chelation by DTPA and the thiol anchorage to the gold NP surface, coupled with a lack of *in vivo* ^{125}I radiolabeling stability, which has been reported previously^{16,17}. Therefore, only the ^{111}In channel was used for later imaging time points.

Two types of tumors with differing MMP9 expression levels (high = A431; low = 4T1Luc; Figure S6) were grown in order to explore the ability of the nanoprobe to report the relative MMP9 activity *in vivo*. By 24 hours, both types of tumors were clearly visible using the ^{111}In imaging channel (Figure S7). Significant tumor accumulation was quantified from the images, corresponding to standardized uptake values (SUVs) of 2.03 ± 0.21 (7.25 ± 0.76 %ID/gram of tissue) and 1.79 ± 0.19 (6.41 ± 0.57 %ID/gram) for the A431 and 4T1Luc tumors, respectively. The multifunctional NPs passively accumulated around the edges of both types of tumors. Further, the heart was still clearly visible at the 24 hour time point, evidence that a significant portion of the NP probe was still circulating in the blood even at this late time point. The NP formulation of the probe was key to this long blood circulation that impeded clearance through the kidney, which occurred for PEG-peptide controls within 4 hours (data not shown), a property that may be advantageous in future drug delivery or imaging applications where sustained presence in the blood is necessary.

By 48 hours, both types of tumors were still visible, and due to a loss of signal in the blood pool, provided significant tumor to muscle ratios of ~8 (Figure 3a and b), which was validated in the biodistribution results (Figure S8). Further, and most interestingly, a significant difference in accumulation was observed between the tumors with high and low MMP9 expression (Figure 3c). Whereas the 4T1Luc tumors with low

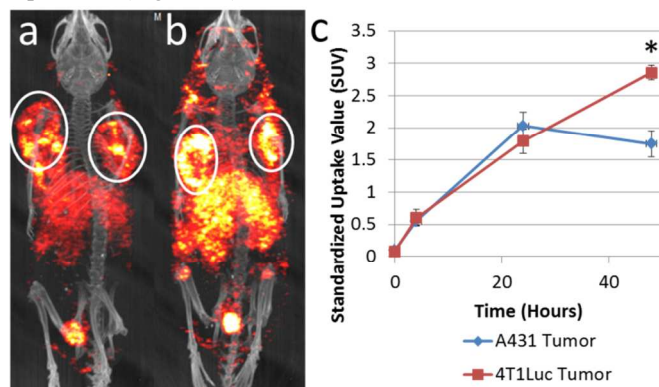


Figure 3. Tumor imaging with dual-radiolabeled nanoparticles. SPECT/CT images of mice with bilateral (a) A431 and (b) 4T1Luc tumors (circled) 48 hours after intravenous injection. (c) Tumor standardized uptake values (SUVs) of ^{111}In over the 48 hours following injection. (* $p < 8.3 \times 10^{-6}$)

MMP9 expression continued to accumulate signal between 24 and 48 hours and reached an SUV of 2.8 ± 0.11 (10.2 ± 0.33 %ID/gram), a decrease in SUV over the same time period to 1.75 ± 0.2 (6.23 ± 0.72 %ID/gram) was observed in the A431 tumors with high MMP9 expression ($p < 8.3 \times 10^{-6}$). It is hypothesized this pharmacokinetic difference in uptake between the two tumor types is a result of their differences in MMP9 expression. More specifically, once the ^{111}In -labeled NPs passively accumulated in tumors, A431 tumors with significant MMP9 expression cleaved the ^{111}In -labeled peptide fragment from the NP, causing clearance from the tumor between 24 and 48 hours. Once again, the NP is central to the success of the strategy, in this case helping to avoid non-specific clearance of uncleaved peptides.

Conclusions

In summary, a gold nanoparticle was radiolabeled with two distinct radionuclides and functionalized with an MMP-cleavable peptide, which was then used as a multispectral SPECT imaging contrast agent *in vivo* to differentiate tumors with differing MMP9 expression. Future work will seek to confirm and expand on targeting MMP activity *in vivo*, incorporate more stable radiochemistry compared to the tyrosine-iodine strategy used in this study in order to integrate ratiometric imaging capability, quantify anchorage stability, and optimize the localized surface plasmon resonant properties of the gold cores for image-guided photothermal therapy.⁵

Methods

Peptide synthesis. Standard Fmoc solid phase synthetic protocols were used to synthesize the peptide containing the MMP9 substrate, tyrosine residue, DTPA chelator, and cysteine anchor (Sequence: DTPA-Gly-Pro-Leu-Gly-Val-Arg-Gly-Lys-Gly-Tyr-Gly-Ahx-Cys-NH₂). Briefly, amino acids were successively loaded onto rink amide resin (0.66 mmol/g resin) using a CEM Discover Liberty Microwave Peptide Synthesizer. The peptide was purified with a Gilson UV/Vis-152 high performance liquid chromatographer (HPLC) using a C18 preparation column. Molecular weight of 1648 g/mol was confirmed with matrix-assisted laser desorption ionization mass spectrometry (MALDI-MS).

Nanoparticle surface modification. 10 mL of 10 nm diameter citrate-stabilized gold nanoparticle suspension (Sigma Aldrich; 6×10^{12} particles/mL) was centrifuged for 1.5 hours at 20.3k g force. Supernatant was removed, and the nanoparticle pellet was resuspended in 5 mL of ultrapure water containing 2.2 mg mPEG-SH (MW5000) and 1 mg of synthesized peptide. After 20 minutes of sonication, the suspension was shaken for 48 hours, and then centrifuged for 1.5 hours at 20.3k g. Supernatant was again removed, 5 mL 0.1 M NH₄OAc (pH 5.5) was added, and suspension was centrifuged for 2 hours at 13.9k g. Supernatant was removed, leaving a 40 μL gold nanoparticle pellet.

In vitro MMP9 experiment. After resuspending the 40 μL peptide-functionalized gold pellet described in the previous section in 10 mL deionized water, a 1 mL aliquot was centrifuged, supernatant decanted, and resuspended in 0.1 M NH₄OAc. 110 μCi ^{64}Cu , provided by the Washington University Cyclotron Facility, was added to the NP pellet and shaken at 45 °C for 1 hour. Radiolabeled NPs were purified from nonchelated ^{64}Cu by centrifugation. Then NP suspensions (1.4 pmol) were incubated with 20 ng MMP9 in 50 μL of PBS for 1.5 hours, after which 450 μL PBS was added and

supernatant was purified from the NPs by centrifugation filtration using a 10k MW filter. Supernatant and NP pellets were counted for radioactivity in a PerkinElmer 1480 Automatic Gamma Counter.

Nanoparticle dual-radiolabeling strategy. 7.1 mCi $^{111}\text{InCl}_3$ (16 μL) was added to the 40 μL peptide-functionalized gold nanoparticle pellet and reacted at 45 °C for 75 minutes. 500 μL PBS was added to the pellet and centrifuged for 2 hours at 20k g. Supernatant was removed, leaving 5.6 mCi of ^{111}In in the pellet. The pellet was then transferred to an iodogen tube and 3.4 mCi Na ^{125}I (50 μL) was added and allowed to react for 1 hour at 25 °C. In preliminary radiolabeling experiments, free ^{125}I was removed in an identical centrifugation process as the ^{111}In , which was confirmed by radio thin layer chromatography (TLC). In the *in vivo* experiment, the dual-labeled nanoparticles were > 98% pure even without a centrifugation after the iodogen reaction. All dually- or singly-labeled constructs used in functional assays were > 95% pure (bound to nanoparticle) as quantified by TLC.

SPECT phantom study. 1 mL of the dual-radiolabeled NP (~100 μCi ^{111}In and 70 μCi ^{125}I) was placed in a 1.5 mL microcentrifuge tube, along with two 1 mL controls containing either only ^{125}I (96 μCi) or only ^{111}In (71 μCi). Tubes were imaged with 16 projection scans (15 seconds per scan) in a NanoSPECT/CT (Bioscan, Inc., Washington, D.C.). Two energy windows were simultaneously tracked in order to detect both ^{111}In and ^{125}I ; 200 ± 60 keV was monitored to track ^{111}In , and 28 ± 3 keV was used to track ^{125}I .

Western blot for MMP9. 4T1Luc tumor and A431 tumor tissues were homogenized using an ultrasonic processor in CHAPS buffer (50mM Pipes/HCl, pH 6.5, 5mM dithiothreitol (DTT), 2mM EDTA, 0.1% Chaps, 20 $\mu\text{g ml}^{-1}$ leupeptin, 10 $\mu\text{g ml}^{-1}$ pepstatin, 10 $\mu\text{g ml}^{-1}$ Aprotinin, 1mM phenyl methylsulphonyl fluoride), and then the tissue lysates were clarified by centrifugation. After protein extraction, the protein concentration was determined by the Bio-Rad Protein assay reagent and the tumor samples were adjusted to an equal amount of protein (50 μg). Gel electrophoresis was performed with Mini-Protean TGX Gel (Bio-Red, Hercules, CA) using the EC120 Mini vertical gel system (Thermo EC, Holbrook, NY). After SDS denaturing electrophoresis, proteins were transferred to PVDF membrane using an EC140 Mini Blot Module (Thermo EC, Holbrook, NY) apparatus. The membrane was blocked 1 hour at room temperature in PBS containing 5% nonfat dry milk (w/v), 0.1% (v/v) Tween-20 (PBS-T), followed by incubation with goat polyclonal anti-MMP-9 (R&D Systems Inc, Minneapolis, MN) primary antibody (0.1 $\mu\text{g/ml}$) in PBS-T containing 3% nonfat dry milk (w/v) at 4 °C overnight. After washing three times for 10 min each in PBS-T, the membrane was incubated for 1 hour with diluted polyclonal rabbit anti-goat IgG conjugated to horseradish peroxidase in PBS-T containing 3% nonfat dry milk (w/v). Membrane was then washed three times for 10 min each in PBS-T and developed using the SuperSignal West Pico chemiluminescent Substrate (Pierce Biotechnology, Rockford, IL) according to the manufacturer's instruction.

Tumor mouse model. All animal studies were performed in compliance with guidelines set forth by the NIH Office of Laboratory Animal Welfare and approved by the Washington University Animal Studies Committee. The A431 (ATCC, Manassas, VA) and 4T1Luc (Sibtech, Brookfield, CT) cells were cultured in Dulbecco's Modified Eagle Medium (DMEM) containing 10% (v/v) fetal bovine serum (Invitrogen, Carlsbad, CA) supplemented with penicillin (100 $\mu\text{g/mL}$) and streptomycin (100 $\mu\text{g/mL}$) in a humidified atmosphere of 5% CO₂ in air. To form

bilateral xenograft tumors (2 tumors per mouse), 10^6 A431 cells in 100 μ L phosphate buffered saline (PBS) were injected into each flank of 12 week old male nude mice weighing 25-30 grams, and tumors were allowed to grow for 18 days. In separate nude mice, 5×10^5 4T1Luc cells in 100 μ L PBS were injected into each flank, and tumors were allowed to grow for 8 days. Average tumor sizes for either type were ~ 100 mm³.

SPECT/CT *in vivo* imaging. 100 μ L of dual radiolabeled gold nanoparticle suspension (~ 0.9 mCi ¹¹¹In and 0.6 mCi ¹²⁵I) was injected via the tail vein of nude mice bearing bilateral tumors (either A431 with high MMP9 expression or 4T1Luc with low MMP9 expression). SPECT/CT imaging was performed on the NanoSPECT/CT. As described in the SPECT phantom study methods above, two energy windows were simultaneously tracked in order to detect both ¹¹¹In and ¹²⁵I. 16 projection scans (60 seconds per scan) were performed immediately after injection, as well as 4 hours, 24 hours, and 48 hours later. Tumor standardized uptake values (SUVs) were quantified from SPECT/CT images using Inveon Research Workspace software (Siemens).

Biodistribution. After the 48 hour time point, animals were sacrificed, and then organs were removed, weighed, and counted for radioactivity in a Wizard Model 1480 gamma counter both immediately after sacrifice and 2 weeks later to isolate signal from both ¹¹¹In and ¹²⁵I.

Supporting Information

Supporting Information is available from the RCS Online Library or from the author.

Acknowledgement

This work supported the National Institutes of Health NHLBI Program of Excellence in Nanotechnology HHSN268201000046 and resources from the Washington University Molecular Imaging Center (NCI P50 CA094056).

Notes and References

1. D. Peer, J. Karp, S. Hong, O. Farokhzad and R. Margalit, *Nat. Nanotechnol.*, 2007, 2, 751-760.
2. X. Huang, P. Jain, I. El-Sayed and M. El-Sayed, *Nanomedicine*, 2007, 2, 681-693.
3. C. Cobley, J. Chen, E. Cho, L. Wang and Y. Xia, *Chem. Soc. Rev.*, 2011, 40, 44-56.
4. Y. Wang, Y. Liu, H. Luehmann, X. Xia, D. Wan, C. Cutler and Y. Xia, *Nano Lett.*, 2013, 13, 581-585.
5. Y. Wang, K. Black, H. Luehmann, W. Li, Y. Zhang, X. Cai, D. Wan, S. Liu, M. Li, P. Kim, Z. Li, L. Wang, Y. Liu and Y. Xia, *ACS Nano*, 2013, 7, 2068-2077.
6. K. Black, J. Yi, J. Rivera and D. Zelasko-Leon, *Nanomedicine*, 2013, 8, 17-28.
7. K. Black, T. Sileika, J. Yi, R. Zhang, J. Rivera and P. Messersmith, *Small*, 2014, 10, 169-178.
8. D. Zeng, N. Lee, Y. Liu, D. Zhou, C. Dence, K. Wooley, J. Katzenellenbogen and M. Welch, *ACS Nano*, 2012, 6, 5209-5219.
9. Y. Wang, Y. Liu, H. Luehmann, X. Xia, P. Brown, C. Jarreau, M. Welch and Y. Xia, *ACS Nano*, 2012, 6, 5880-5888.

10. Y. Zhao, D. Sultan, L. Detering, S. Cho, G. Sun, R. Pierce, K. Wooley and Y. Liu, *Angew. Chem. Int. Ed.*, 2014, 53, 156-159.
11. K. Black, Y. Wang, H. Luehmann, X. Cai, W. Xing, B. Pang, Y. Zhao, C. Cutler, L. Wang, Y. Liu and Y. Xia, *ACS Nano*, 2014, 8, 4385-4394.
12. H. Lee, W. Akers, W. Edwards, K. Liang, P. Cheney, J. Culver and S. Achilefu, *Journal of Biomedical Optics*, 2009, 14, 040507-040501.
13. E. Olson, T. Jiang, T. Aguilera, Q. Nguyen, L. Ellies, M. Scadeng and R. Tsien, *Proc. Natl. Acad. Sci. U.S.A.*, 2010, 107, 4311-4316.
14. M. Solomon, K. Guo, G. Sudlow, M. Berezin, W. Edwards, S. Achilefu and W. Akers, *Journal of Biomedical Optics*, 2011, 16, 066019-066011.
15. E. Mebrahtu, A. Zheleznyak, M. Hur, R. Laforest and S. Lapi, *Nuclear Medicine and Biology*, 2013, 40, 190-196.
16. L. Shih, S. Thorpe, G. Griffiths, H. Diril, G. Ong, H. Hansen, D. Goldenberg and M. Mattes, *J. Nucl. Med.*, 1994, 35, 899-908.
17. R. Stein, S. Govindan, M. Mattes, S. Chen, L. Reed, G. Newsome, B. McBride, G. Griffiths, H. Hansen and D. Goldenberg, *Cancer Res.*, 2003, 63, 111-118.